

ECGFlowCMR: Pretraining with ECG-Generated Cine CMR Helps Cardiac Disease Classification and Phenotype Prediction

Xiaocheng Fang*	Zhengyao Ding*	Guangkun Nie*	Jieyi Cai
School of Intelligence Science and Technology, Peking University Beijing, China	College of Computer Science and Technology, Zhejiang University Zhejiang, China	School of Intelligence Science and Technology, Peking University Beijing, China	University of Chinese Academy of Sciences Beijing, China
Yujie Xiao	Bo Liu	Jiarui Jin	Haoyu Wang
National Institute of Health Data Science, Peking University Beijing, China	School of Intelligence Science and Technology, Peking University Beijing, China	School of Intelligence Science and Technology, Peking University Beijing, China	University of Chinese Academy of Sciences Beijing, China
Shun Huang	Ting Chen	Hongyan Li†	Shenda Hong†
National Institute of Health Data Science, Peking University Beijing, China	The First Affiliated Hospital of Zhejiang University School of Medicine Zhejiang, China	School of Intelligence Science and Technology, Peking University Beijing, China	National Institute of Health Data Science, Peking University Beijing, China

Abstract

Cardiac Magnetic Resonance (CMR) imaging provides a comprehensive assessment of cardiac structure and function but remains constrained by high acquisition costs and reliance on expert annotations, limiting the availability of large-scale labeled datasets. In contrast, electrocardiograms (ECGs) are inexpensive, widely accessible, and offer a promising modality for conditioning the generative synthesis of cine CMR. To this end, we propose ECGFlowCMR, a novel ECG-to-CMR generative framework that integrates a Phase-Aware Masked Autoencoder (PA-MAE) and an Anatomy-Motion Disentangled Flow (AMDF) to address two fundamental challenges: (1) the cross-modal temporal mismatch between multi-beat ECG recordings and single-cycle CMR sequences, and (2) the anatomical observability gap due to the limited structural information inherent in ECGs. Extensive experiments on the UK Biobank and a proprietary clinical dataset demonstrate that ECGFlowCMR can generate realistic cine CMR sequences from ECG inputs, enabling scalable pretraining and improving performance on downstream cardiac disease classification and phenotype prediction tasks. The code is available at <https://github.com/PKUDigitalHealth/ECGFlowCMR>.

*These authors contributed equally to this research.

†Corresponding authors.

Permission to make digital or hard copies of all or part of this work for personal or classroom use is granted without fee provided that copies are not made or distributed for profit or commercial advantage and that copies bear this notice and the full citation on the first page. Copyrights for components of this work owned by others than the author(s) must be honored. Abstracting with credit is permitted. To copy otherwise, or republish, to post on servers or to redistribute to lists, requires prior specific permission and/or a fee. Request permissions from permissions@acm.org.

KDD '26, Jeju, Korea

© 2018 Copyright held by the owner/author(s). Publication rights licensed to ACM.
ACM ISBN 978-1-4503-XXXX-X/18/06
<https://doi.org/XXXXXX.XXXXXXX>

CCS Concepts

- Applied computing → Health informatics; • Computing methodologies → Artificial intelligence.

Keywords

ECG-to-CMR Generation, Cross-Modal Synthesis, Phase Awareness, Anatomy-Motion Disentanglement, Generative Pretraining

ACM Reference Format:

Xiaocheng Fang, Zhengyao Ding, Guangkun Nie, Jieyi Cai, Yujie Xiao, Bo Liu, Jiarui Jin, Haoyu Wang, Shun Huang, Ting Chen, Hongyan Li, and Shenda Hong. 2018. ECGFlowCMR: Pretraining with ECG-Generated Cine CMR Helps Cardiac Disease Classification and Phenotype Prediction. In *Proceedings of the 32nd ACM SIGKDD Conference on Knowledge Discovery and Data Mining (KDD '26)*. ACM, New York, NY, USA, 9 pages. <https://doi.org/XXXXXX.XXXXXXX>

1 Introduction

Cardiac Magnetic Resonance (CMR) imaging is a pivotal noninvasive modality for the comprehensive assessment of cardiac structure and function [3, 37]. However, the development of AI models for automated CMR analysis is hindered by the scarcity of large-scale, expertly annotated datasets. Although the UK Biobank (UKB) [6] provides 42,129 CMR scans, this scale remains significantly below the sample size (typically on the order of 10^5 to 10^6) required to pretrain robust foundation models [1, 22]. The substantial cost and annotation burden associated with CMR acquisition have so far precluded the release of larger public datasets, thereby limiting the generalizability and clinical utility of AI-based methods. In this context, generative modeling has emerged as a promising approach to synthesize realistic CMR data at scale, mitigating data scarcity and enhancing model performance.

Recent progress in generative modeling has enabled high-fidelity synthesis across various medical imaging modalities, such as chest

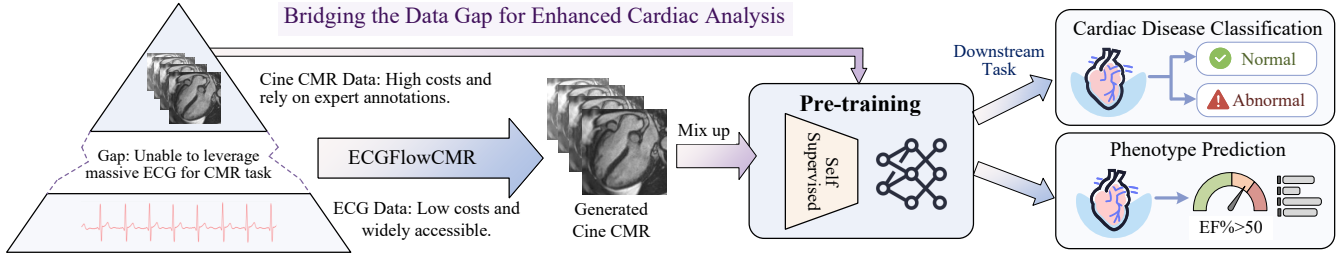


Figure 1: Overview of the generative pretraining paradigm. Unlike conventional methods that depend on limited annotated CMR data, ECGFlowCMR leverages available ECG signals to synthesize realistic cine CMR sequences. This enables scalable pretraining and improves performance on downstream tasks, including cardiac disease classification and phenotype prediction.

X-rays [5, 25], 3D brain MRIs [24, 29], and echocardiographic videos [7, 17], thereby improving representation learning and downstream task performance. However, cine CMR synthesis remains comparatively underexplored. Existing methods exhibit notable limitations: DragNet [39] relies on static-frame conditioning, which undermines temporal coherence, while CPGG [18] depends on phenotype labels extracted from CMR segmentation, introducing annotation dependency and limiting scalability. These issues highlight the need for flexible, annotation-independent generative frameworks for cine CMR synthesis. Given the limited availability and high acquisition cost of CMR data, synthesizing cine CMR sequences from electrocardiograms (ECGs) represents a promising and scalable alternative. ECGs are inexpensive, widely accessible, and routinely collected in both clinical practice and population-scale screening. Furthermore, ECGs capture electrophysiological signals correlated with cardiac structure and function [40], offering a physiologically grounded proxy for data-driven cine modeling. Preliminary work includes a cross-modal autoencoder [26] that learns a shared latent space for cine sequence imputation, and CardioNets [10], which employs masked autoregression to generate latent CMR representations. These studies demonstrate the feasibility of ECG-conditioned cine CMR synthesis and motivate the development of more expressive and generalizable models.

However, ECG-to-CMR synthesis faces two key challenges: 1) **Cross-modal temporal mismatch:** A 10-second ECG captures multi-beat electrophysiological dynamics with variable heart rates, whereas a 50-frame cine CMR typically represents a single, phase-resolved cardiac cycle. This discrepancy renders temporal alignment and beat-to-cycle correspondence inherently ambiguous, complicating sequence generation. 2) **Anatomical observability gap:** As ECG primarily reflects surface-level electrical activity rather than structural morphology, it imposes only weak constraints on cardiac anatomy and image appearance. This under-constrained mapping often results in synthetic CMRs that capture coarse motion patterns but fail to reconstruct fine-grained anatomical details.

To overcome these limitations, we propose ECGFlowCMR, a generative framework that integrates a Phase-Aware Masked Autoencoder (PA-MAE) and an Anatomy-Motion Disentangled Flow (AMDF) module. PA-MAE learns ECG representations under joint supervision of signal reconstruction and cardiac-phase prediction, where a dedicated phase head identifies complete cardiac cycles to enable temporal alignment with cine CMR sequences. AMDF

constructs a time-invariant anatomical prior via a 3D variational autoencoder (3D-VAE), generating a static latent template as a structural anchor. Conditioned on this template and an initial motion state, a Diffusion Transformer (DiT)-based flow-matching network predicts ECG-conditioned velocity fields to synthesize anatomically accurate and temporally coherent motion. Experiments on the UK Biobank and a proprietary clinical dataset demonstrate that ECGFlowCMR generates realistic cine CMR sequences from ECG inputs, facilitates scalable pretraining, and enhances performance on downstream cardiac analysis tasks. The main contributions of this work are summarized as follows:

- We propose ECGFlowCMR, a novel ECG-to-CMR generative framework designed for scalable pretraining and downstream cardiac analysis tasks. It addresses two major limitations of prior approaches: the cross-modal temporal mismatch and the anatomical observability gap.
- The proposed PA-MAE module enables cycle-level alignment between multi-beat ECG signals and single-cycle cine CMR by modeling cardiac phase dynamics, while the AMDF module improves anatomical plausibility by disentangling static structure from dynamic motion in the latent space.
- Extensive experiments on the UK Biobank dataset demonstrate that ECGFlowCMR synthesizes high-fidelity cine CMR and improves downstream disease classification and phenotype prediction when used for synthetic pretraining.
- To evaluate generalizability, we further curate a proprietary clinical dataset of 535 patients for cardiomyopathy classification. Results on this external benchmark confirm our method’s robustness under real-world distribution shifts in patient demographics and clinical acquisition settings.

2 Related Work

2.1 Video Generation

Video generation has progressed from direct pixel-level synthesis to scalable latent sequence modeling, which maintains spatial fidelity and temporal coherence. Early GAN-based models, including VGAN [34], TGAN [27], and MoCoGAN [30], captured short-term dynamics but exhibited limited scalability due to recursive error accumulation and the challenges of high-dimensional spatiotemporal modeling. A prevalent approach involves generation within a compressed latent space, which reduces visual redundancy and

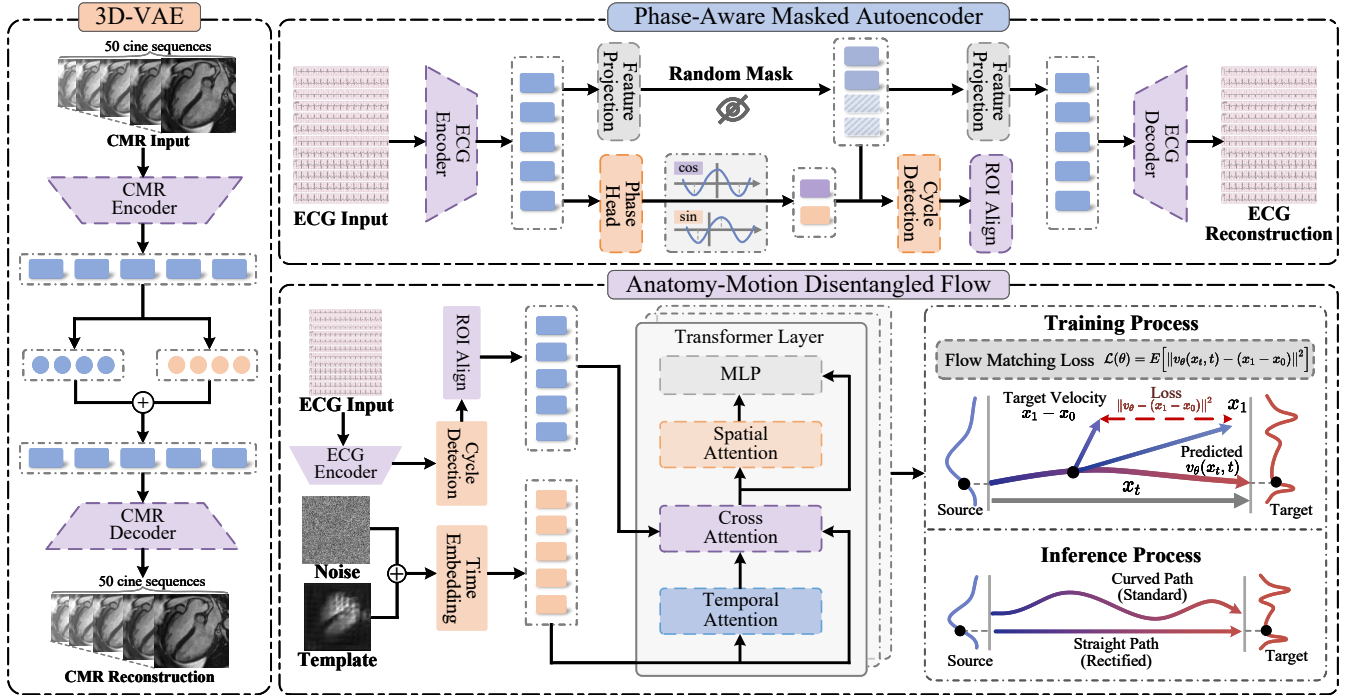


Figure 2: Illustration of the proposed ECGFlowCMR for generating realistic cine CMR sequences from 12-lead ECGs. The framework consists of two components: PA-MAE learns phase-aware, cycle-aligned ECG representations to provide conditioning features that reduce temporal misalignment between ECG and CMR. AMDF conducts anatomy-motion disentangled latent flow matching to synthesize anatomically faithful and temporally coherent cine sequences.

improves temporal modeling efficiency. Stochastic latent-variable methods further mitigate pixel-level complexity and enable long-horizon prediction [2, 9]. Token-based techniques discretize frames or spatiotemporal patches via vector-quantized encoders, facilitating Transformer-based autoregression, masked modeling, and hierarchical planning [32, 33, 38]. Diffusion models have recently demonstrated superior perceptual quality through iterative denoising with temporal coupling [15], while their latent-space variants significantly enhance sample fidelity and reduce computational cost [4, 13]. Current trends converge toward hybrid architectures that integrate continuous or discrete latent compression with expressive temporal backbones, such as Transformers or diffusion models. These architectures increasingly incorporate conditioning signals (e.g., text, actions) to improve controllability and ensure long-range temporal consistency [15, 28, 33].

2.2 CMR Video Generation

Cine CMR generation aims to produce temporally coherent sequences with anatomically accurate structures and physiologically realistic motion. Early methods adopt explicit motion modeling by warping a static reference frame using estimated deformation fields. DragNet [39] exemplifies this paradigm by integrating spatiotemporal registration with generative modeling. More recent approaches shift toward implicit distribution learning with cardiac priors. GANcMRI [35] introduces latent prompting to control morphological and functional attributes, while diffusion-based models

improve perceptual fidelity and motion realism via disease-aware 4D synthesis [19] and latent or patch-wise strategies that balance quality and efficiency [16]. In parallel, CMR-to-CMR translation under weak or unpaired supervision transfers motion and anatomical priors across modalities. Representative methods include tagged-to-cine synthesis using spatiotemporal Transformers [21] and unpaired DENSE-to-cine generation via motion-guided diffusion [8]. However, these approaches require modality-specific CMR inputs at inference, limiting scalability. Trait-conditioned generators alleviate this constraint by synthesizing cine sequences from structured cardiac phenotypes (e.g., CPGG [18]), though their performance depends on reliable phenotype extraction. To remove CMR dependency altogether, cross-modal frameworks generate cine sequences from ECG signals. One strategy aligns ECG and CMR representations in a shared latent space [26], enabling direct ECG-to-cine synthesis. CardioNets [10] extends this paradigm via masked autoregressive decoding. Despite encouraging progress, ECG-conditioned generation remains challenged by temporal misalignment and limited anatomical observability.

3 Methodology

3.1 Phase-Aware Masked Autoencoder

To extract semantically rich and rhythm-aware representations from 12-lead ECGs, we propose the Phase-Aware Masked Autoencoder (PA-MAE). Trained with dual supervision, PA-MAE facilitates

robust morphological representation learning and enables precise temporal alignment with cine CMR sequences.

Masked Signal Reconstruction. As illustrated in Figure 2, PA-MAE adopts a standard masked autoencoder [12] for self-supervised ECG representation learning. Given an input $x_{\text{ecg}} \in \mathbb{R}^{C \times T}$, where C denotes the number of leads and T the temporal length, the encoder E_{ecg} extracts semantic features as $F = E_{\text{ecg}}(x_{\text{ecg}})$. To promote robust feature learning, a proportion ρ of temporal positions is randomly masked by zeroing out the corresponding feature vectors:

$$F_{\text{masked}} = F \odot m, \quad (1)$$

where $m \in \{0, 1\}^{T'}$ is a binary mask containing a fraction ρ of zeros, T' denotes the encoded temporal length, and \odot represents element-wise multiplication. The masked features F_{masked} are then passed through a decoder D_{ecg} to reconstruct the original ECG signal. Specifically, the reconstruction is given by $\hat{x}_{\text{ecg}} = D_{\text{ecg}}(F_{\text{masked}})$, where \hat{x}_{ecg} denotes the predicted signal corresponding to the input. The model is trained to minimize the mean squared error (MSE) between the input and the reconstructed signal:

$$\mathcal{L}_{\text{rec}} = \frac{1}{CT} \|\hat{x}_{\text{ecg}} - x_{\text{ecg}}\|_2^2, \quad (2)$$

which encourages the model to capture meaningful morphological patterns without requiring manual annotations.

Phase-Aware Temporal Supervision. Beyond masked signal reconstruction, we propose a dedicated phase prediction head P_{ecg} to explicitly model cardiac rhythm and mitigate temporal misalignment between ECG signals and CMR sequences. The module P_{ecg} operates on the full set of unmasked encoder features and outputs sinusoidal representations of the cardiac phase:

$$\hat{\phi} = P_{\text{ecg}}(F) = [\sin(\phi), \cos(\phi)], \quad (3)$$

where $\phi \in [0, 2\pi]$ denotes the normalized phase within each cardiac cycle. Ground-truth phase labels ϕ_{gt} are computed via R-peak detection from Lead II and linearly interpolated across each R-R interval. The phase prediction loss is followed:

$$\mathcal{L}_{\text{phase}} = \frac{1}{T'} \|\hat{\phi} - \phi_{\text{gt}}\|_2^2. \quad (4)$$

Here, T' denotes the encoded temporal length. To achieve temporal alignment between ECG and cine CMR, complete cardiac cycles are extracted from the predicted phase sequence and resampled using ROI Align into 50-frame representations, matching the temporal resolution of cine CMR.

Training Objective. The overall training objective combines both reconstruction and phase prediction losses:

$$\mathcal{L}_{\text{PA-MAE}} = \mathcal{L}_{\text{rec}} + \mathcal{L}_{\text{phase}}. \quad (5)$$

This dual-supervision strategy ensures that the learned features retain both morphological and temporal semantics critical for downstream CMR synthesis.

3.2 Anatomy-Motion Disentangled Flow

To address the anatomical observability gap where ECG signals impose weak constraints on cardiac morphology, we propose the Anatomy-Motion Disentangled Flow (AMDF), which explicitly disentangles static anatomical structure from dynamic temporal

motion in a latent space. Specifically, AMDF first extracts a time-invariant anatomical representation using a 3D variational autoencoder (3D-VAE), and subsequently models the time-dependent motion residual via a conditional flow-matching network.

Anatomical Anchor Learning. We employ a 3D-VAE to encode CMR videos into a latent space using an anisotropic compression strategy that reduces spatial resolution while preserving temporal fidelity. Given a CMR video $x_{\text{cmr}} \in \mathbb{R}^{C \times T \times H \times W}$, where C denotes the input channel and T the number of frames, the encoder E_{cmr} maps x_{cmr} to a latent representation $\mathbf{z} = E_{\text{cmr}}(x_{\text{cmr}})$, where $\mathbf{z} \in \mathbb{R}^{C' \times T \times H' \times W'}$, with C' indicating the latent channel dimension and $H' \times W'$ the spatially downsampled resolution. The decoder D_{cmr} then reconstructs the input as $\hat{x}_{\text{cmr}} = D_{\text{cmr}}(\mathbf{z})$.

After training the 3D-VAE, we extract latent representations from all training CMR videos and compute a static anatomical template by averaging over both the sample and temporal dimensions:

$$\mathbf{z}_{\text{template}} = \frac{1}{NT} \sum_{i=1}^N \sum_{t=1}^T \mathbf{z}_{i,t}, \quad (6)$$

where N denotes the number of training subjects and T the number of frames per sample. The resulting template representation $\mathbf{z}_{\text{template}}$ captures the average anatomical structure across the training population and serves as a structural prior encoding population-level cardiac morphology.

Conditional Flow Matching. To model time-varying cardiac motion in a physiologically coherent manner, we adopt a conditional flow-matching framework built upon a Diffusion Transformer (DiT) [20, 23]. Conditioned on a static anatomical template and an initial motion state, the network learns a continuous velocity field that governs latent-space dynamics. Specifically, we define a velocity field $v_{\theta}(\mathbf{z}_t, t, c)$ that predicts the instantaneous motion at an intermediate time $t \in [0, 1]$, where \mathbf{z}_t denotes the interpolated latent representation at time t , and c represents ECG-derived conditioning features extracted by the PA-MAE encoder.

During training, we simulate latent motion trajectories by sampling time points $t \sim U(0, 1)$ and linearly interpolating between a noise-perturbed anatomical anchor \mathbf{z}_0 and the target CMR latent representation \mathbf{z}_1 :

$$\mathbf{z}_t = (1 - t) \cdot \mathbf{z}_0 + t \cdot \mathbf{z}_1, \quad (7)$$

where the noise-perturbed anatomical anchor \mathbf{z}_0 is defined as:

$$\mathbf{z}_0 = \mathbf{z}_{\text{template}} + \alpha \cdot \boldsymbol{\epsilon}, \quad \boldsymbol{\epsilon} \sim \mathcal{N}(0, \mathbf{I}). \quad (8)$$

Here, \mathbf{z}_1 is the latent representation of the target CMR sequence obtained from the 3D-VAE encoder, and α controls the level of noise injection to the anatomical prior.

The ground-truth velocity field $\mathbf{v}_{\text{true}} = \mathbf{z}_1 - \mathbf{z}_0$ defines a constant linear drift from the initial to the target state. The DiT-based network v_{θ} is trained to regress this velocity, conditioned on the interpolated latent \mathbf{z}_t , the corresponding time step t , and the ECG-derived context c :

$$\hat{\mathbf{v}} = v_{\theta}(\mathbf{z}_t, t, c). \quad (9)$$

The training objective minimizes the expected mean squared error (MSE) between the predicted and ground-truth velocity fields:

$$\mathcal{L}_{\text{AMDF}} = \mathbb{E}_{t, \mathbf{z}_0, \mathbf{z}_1, c} [\|\hat{\mathbf{v}} - (\mathbf{z}_1 - \mathbf{z}_0)\|_2^2]. \quad (10)$$

Table 1: Comparison with generative approaches on the UKB dataset.

Methods	Ref.	LPIPS↓	FID↓	FVD↓	Inference time↓
VideoGPT [38]	ArXiv'21	0.35	107.41	24.99	2.15 sec / vid.
ModelScopeT2V [36]	ArXiv'23	0.37	104.19	31.43	3.87 sec / vid.
Cross-Modal Autoencoder [26]	Nat. Commun.'23	0.32	99.24	28.62	0.63 sec / vid.
EchoPulse [17]	ICLR'25	0.31	85.80	21.41	0.84 sec / vid.
CardioNets [10]	NEJM AI'26	0.28	89.83	21.65	4.33 sec / vid.
ECGFlowCMR	Ours	0.27	37.28	14.41	0.45 sec / vid.
Increased	-	3.57%↑	56.56%↑	32.70%↑	28.57%↑

This objective encourages the network to learn phase-aware latent trajectories that maintain anatomical consistency and temporal coherence, thereby enabling realistic cardiac motion synthesis.

Inference and Sampling. At inference time, we synthesize cine CMR latents by numerically integrating the learned velocity field from an initial latent state z_0 toward the target latent z_1 . Starting from the anatomical template perturbed with noise, we iteratively update the latent using an explicit Euler scheme:

$$z_{t+\Delta t} = z_t + \Delta t \cdot v_\theta(z_t, t, c). \quad (11)$$

Here, Δt denotes the integration step size and v_θ is the DiT-based conditional velocity field. The integration is performed from $t = 0$ to $t = 1$, yielding the final latent representation z_1 . This latent is then decoded by the 3D-VAE decoder to generate the corresponding cine CMR sequence.

By jointly refining anatomical structure via the anatomical anchor and synthesizing ECG-guided temporal motion through conditional flow matching, AMDF generates cardiac dynamics that are anatomically plausible and temporally coherent, effectively mitigating the anatomical observability gap between ECG signals and cardiac morphology.

4 Experiments

4.1 Datasets and Evaluation Metrics

We conducted experiments on two datasets: a large-scale public dataset from the UK Biobank (UKB) and a proprietary clinical dataset curated for cardiomyopathy diagnosis from the Affiliated Hospital of Zhejiang University, referred to as ZJU-CM. These datasets were used to evaluate both in-distribution performance and out-of-distribution generalization. All classification tasks were assessed using five-fold cross-validation. Evaluation metrics included LPIPS [41], FID [14], FVD [31], and inference time.

UKB Dataset. We evaluated our ECGFlowCMR on 42,129 four-chamber cine CMR sequences from the UKB, each paired with a corresponding 12-lead ECG. To avoid subject overlap, the data were split at the patient level into 29,490 training, 4,212 validation, and 8,427 testing samples. Two downstream tasks were defined. For cardiac disease classification, we constructed three balanced cohorts with equal numbers of positive and negative cases: coronary artery disease (UKB-CAD, $n = 5,464$), cardiomyopathy (UKB-CM, $n = 196$), and heart failure (UKB-HF, $n = 578$). For cardiac phenotype prediction, we further subset the above split into 19,487 training, 2,758 validation, and 5,553 testing samples, each annotated with

82 phenotypes following the UKB imaging protocol [3]. This dual-task setup facilitates comprehensive evaluation of both diagnostic classification and quantitative phenotype regression, aligning with the practical demands of automated cardiac image interpretation.

ZJU-CM Dataset. The ZJU-CM dataset was collected from the Affiliated Hospital of Zhejiang University and consists of 535 patients. It was curated for cardiomyopathy classification and comprises four diagnostic groups: 195 patients with hypertrophic cardiomyopathy (HCM), 160 with dilated cardiomyopathy (DCM), 33 with restrictive cardiomyopathy (RCM), and 147 healthy controls. ZJU-CM was used to evaluate two classification tasks: (i) binary classification of cardiomyopathy versus control, and (ii) multi-class classification of cardiomyopathy subtypes.

4.2 Implementation Details and Baselines

For data preprocessing, we utilized the UKB segmentation model [3] to extract cardiac regions and uniformly resized all cine CMR sequences to a spatial resolution of $1 \times 50 \times 96 \times 96$. A 3D-VAE was trained with an $8\times$ spatial compression ratio to encode CMR videos. Simultaneously, our PA-MAE processed 12-lead ECG signals comprising 5,000 timepoints, employing $8\times$ temporal downsampling and a random masking ratio of 0.5. The AMDF module was trained for 10 epochs using the AdamW optimizer with a learning rate of 1×10^{-4} , weight decay of 1×10^{-4} , and batch size of 4. Downstream diagnostic models were fine-tuned for 100 epochs. All experiments were conducted on an NVIDIA A100 GPU.

We compared our method with four state-of-the-art baselines: VideoGPT [38], a vector-quantized autoregressive model for video generation; ModelScopeT2V [36], a diffusion-based framework for text-to-video synthesis; EchoPulse [17], a discrete token-based masked modeling framework for ECG-to-echocardiogram generation; and CardioNets [10], a masked autoregressive framework for ECG-to-CMR translation. We additionally included a cross-modal autoencoder [26] that reconstructs CMR sequences from ECGs as a deterministic baseline. However, its inherent one-to-one mapping precludes the modeling of stochastic variations, making it unsuitable for generative pretraining and downstream data augmentation.

4.3 Comparisons with State-of-The-Arts

Evaluation on CMR Generation Quality. As shown in Table 1, ECGFlowCMR surpasses five state-of-the-art baselines across all evaluation metrics on the UKB dataset, establishing its superiority in perceptual quality, distributional alignment, and computational efficiency. It achieves the lowest LPIPS (0.27), indicating

Table 2: Comparison of different methods on cardiac disease classification.

Methods	Ref.	UKB-CAD		UKB-CM		UKB-HF	
		ACC↑	AUC↑	ACC↑	AUC↑	ACC↑	AUC↑
ViT [11]	ICLR'21	0.662 \pm 0.014	0.714 \pm 0.022	0.705 \pm 0.008	0.747 \pm 0.032	0.708 \pm 0.038	0.779 \pm 0.018
MAE [12](real)	CVPR'22	0.695 \pm 0.086	0.743 \pm 0.048	0.776 \pm 0.017	0.806 \pm 0.054	0.776 \pm 0.032	0.854 \pm 0.016
<i>Training with 100% Mixed Synthetic Data</i>							
VideoGPT [38]	ArXiv'21	0.697 \pm 0.045	0.752 \pm 0.021	0.779 \pm 0.051	0.809 \pm 0.038	0.781 \pm 0.025	0.857 \pm 0.012
ModelScopeT2V [36]	ArXiv'23	0.701 \pm 0.031	0.761 \pm 0.052	0.784 \pm 0.024	0.811 \pm 0.042	0.784 \pm 0.054	0.859 \pm 0.031
EchoPulse [17]	ICLR'25	0.709 \pm 0.012	0.778 \pm 0.035	0.799 \pm 0.007	0.828 \pm 0.048	0.798 \pm 0.032	0.868 \pm 0.019
CardioNets [10]	NEJM AI'26	0.706 \pm 0.054	0.769 \pm 0.018	0.792 \pm 0.037	0.819 \pm 0.014	0.791 \pm 0.009	0.861 \pm 0.045
ECGFlowCMR	Ours	0.716\pm0.027	0.787\pm0.011	0.806\pm0.035	0.837\pm0.024	0.808\pm0.018	0.876\pm0.026
Increased	-	0.99%↑	1.16%↑	0.88%↑	1.09%↑	1.25%↑	0.92%↑
<i>Training with 200% Mixed Synthetic Data</i>							
VideoGPT [38]	ArXiv'21	0.699 \pm 0.028	0.765 \pm 0.044	0.788 \pm 0.019	0.815 \pm 0.052	0.789 \pm 0.041	0.856 \pm 0.025
ModelScopeT2V [36]	ArXiv'23	0.705 \pm 0.051	0.774 \pm 0.015	0.796 \pm 0.044	0.823 \pm 0.031	0.797 \pm 0.012	0.864 \pm 0.053
EchoPulse [17]	ICLR'25	0.717 \pm 0.014	0.789 \pm 0.058	0.810 \pm 0.053	0.839 \pm 0.029	0.811 \pm 0.026	0.878 \pm 0.014
CardioNets [10]	NEJM AI'26	0.711 \pm 0.036	0.782 \pm 0.027	0.804 \pm 0.022	0.831 \pm 0.015	0.804 \pm 0.048	0.871 \pm 0.037
ECGFlowCMR	Ours	0.723\pm0.019	0.796\pm0.028	0.818\pm0.013	0.845\pm0.039	0.817\pm0.030	0.886\pm0.021
Increased	-	0.84%↑	0.89%↑	0.99%↑	0.72%↑	0.74%↑	0.91%↑
<i>Training with 300% Mixed Synthetic Data</i>							
VideoGPT [38]	ArXiv'21	0.709 \pm 0.034	0.776 \pm 0.051	0.798 \pm 0.042	0.825 \pm 0.016	0.800 \pm 0.054	0.863 \pm 0.032
ModelScopeT2V [36]	ArXiv'23	0.714 \pm 0.047	0.783 \pm 0.023	0.805 \pm 0.014	0.833 \pm 0.051	0.807 \pm 0.021	0.870 \pm 0.044
EchoPulse [17]	ICLR'25	0.723 \pm 0.052	0.797 \pm 0.013	0.818 \pm 0.028	0.848 \pm 0.054	0.820 \pm 0.012	0.884 \pm 0.036
CardioNets [10]	NEJM AI'26	0.718 \pm 0.025	0.790 \pm 0.048	0.812 \pm 0.033	0.841 \pm 0.027	0.813 \pm 0.045	0.877 \pm 0.019
ECGFlowCMR	Ours	0.730\pm0.011	0.804\pm0.033	0.826\pm0.020	0.854\pm0.014	0.826\pm0.028	0.891\pm0.016
Increased	-	0.97%↑	0.88%↑	0.98%↑	0.71%↑	0.73%↑	0.79%↑

enhanced perceptual similarity to the ground truth. In addition, ECGFlowCMR substantially lowers the FID to 37.28 and FVD to 14.41, yielding relative improvements of 56.56% and 32.70%, respectively, over the strongest baseline. Additionally, it delivers the fastest inference time of 0.45 seconds per video, which constitutes a 28.57% reduction relative to EchoPulse and up to a 90% reduction compared to ModelScopeT2V. While the cross-modal autoencoder achieves competitive inference speed (0.63s), its deterministic nature limits generative diversity, resulting in inferior performance on LPIPS (0.32), FID (99.24), and FVD (28.62). These findings collectively underscore the effectiveness of ECGFlowCMR in synthesizing cine CMR sequences that are both high-fidelity and efficient, making it well-suited for generative pretraining and downstream clinical applications.

Evaluation on Cardiac Disease Classification. Table 2 reports classification performance on three UKB disease cohorts (UKB-CAD, UKB-CM, and UKB-HF) under 100%, 200%, and 300% mixed synthetic-data settings. ECGFlowCMR consistently achieves the highest accuracy (ACC) and area under the ROC curve (AUC) across all disease categories and data augmentation ratios. Notably, under the 100% synthetic-data setting, ECGFlowCMR achieves ACC/AUC scores of 0.716/0.787 on UKB-CAD, 0.806/0.837 on UKB-CM, and 0.808/0.876 on UKB-HF, surpassing the strongest baseline by a substantial margin. As the synthetic data proportion increases to 200% and 300%, ECGFlowCMR demonstrates monotonic improvements in classification performance. These consistent gains across all cohorts indicate that the synthetic CMR sequences generated

by ECGFlowCMR are both high-quality and clinically informative, thereby enhancing downstream disease classification.

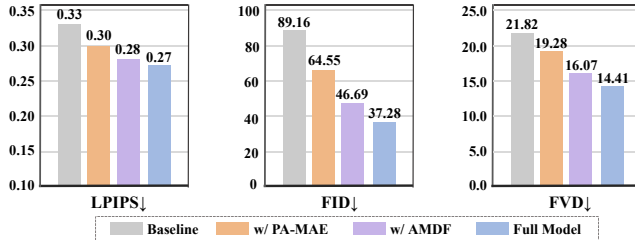
Evaluation on Cardiac Phenotype Prediction. Table 3 reports regression results on four representative cardiac phenotypes (LVEDV, LVEF, LVM, and RVEDV) as well as the average performance across 82 phenotypic traits under 100%, 200%, and 300% synthetic-data mixing settings. ECGFlowCMR consistently achieves the lowest mean absolute error (MAE) and the highest coefficient of determination (R^2) across all configurations. Under the 100% synthetic-data condition, ECGFlowCMR attains an overall R^2 of 0.470, exceeding the strongest baseline (EchoPulse, $R^2 = 0.454$). As the proportion of synthetic data increases, the model further improves to an R^2 of 0.499, yielding a relative gain of 5.94%. These consistent and substantial improvements across diverse phenotypic traits underscore the generative fidelity of ECGFlowCMR and its effectiveness in enhancing downstream phenotype prediction.

4.4 Ablation Studies

In the ablation studies, we systematically assess the contribution of each module within ECGFlowCMR using the UKB dataset. As illustrated in Figure 3, both PA-MAE and AMDF are essential for high-fidelity cine CMR synthesis. The performance degradation observed in the “ECGFlowCMR w/o PA-MAE” variant highlights the critical role of phase-aware ECG representation learning in capturing cycle-aligned morphological features. Likewise, the reduced performance in “ECGFlowCMR w/o AMDF” underscores the

Table 3: Comparison of different methods on cardiac phenotype prediction.

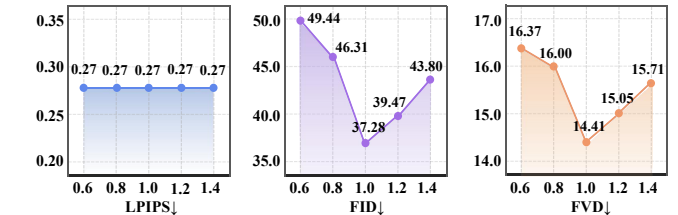
Methods	Ref.	LVEDV		LVEF		LVM		RVEDV		Overall
		MAE↓	R ² ↑	MAE↓	R ² ↑	MAE↓	R ² ↑	MAE↓	R ² ↑	
ViT [11]	ICLR'21	11.52	0.772	3.75	0.367	7.56	0.763	13.14	0.770	0.417
MAE [12] (real)	CVPR'22	11.35	0.769	3.67	0.412	6.67	0.801	12.62	0.784	0.441
<i>Training with 100% Mixed Synthetic Data</i>										
VideoGPT [38]	ArXiv'21	11.20	0.773	3.54	0.415	6.48	0.805	12.47	0.786	0.445
ModelScopeT2V [36]	ArXiv'23	11.28	0.771	3.51	0.418	6.51	0.808	12.40	0.790	0.443
EchoPulse [17]	ICLR'25	10.83	0.785	3.44	0.427	6.25	0.818	12.16	0.802	0.454
CardioNets [10]	NEJM AI'26	10.97	0.782	3.47	0.423	6.32	0.814	12.25	0.799	0.451
ECGFlowCMR	Ours	10.40	0.806	3.41	0.436	6.14	0.828	11.92	0.809	0.470
Increased	-	3.97%↑	2.68%↑	0.87%↑	2.11%↑	1.76%↑	1.22%↑	1.97%↑	0.87%↑	3.52%↑
<i>Training with 200% Mixed Synthetic Data</i>										
VideoGPT [38]	ArXiv'21	11.24	0.774	3.51	0.417	6.44	0.806	12.49	0.789	0.447
ModelScopeT2V [36]	ArXiv'23	11.25	0.773	3.45	0.421	6.35	0.812	12.27	0.795	0.452
EchoPulse [17]	ICLR'25	10.69	0.795	3.40	0.433	6.14	0.821	11.89	0.806	0.463
CardioNets [10]	NEJM AI'26	10.82	0.791	3.43	0.429	6.24	0.817	12.04	0.803	0.459
ECGFlowCMR	Ours	10.19	0.812	3.39	0.441	5.92	0.836	11.53	0.821	0.482
Increased	-	4.68%↑	2.14%↑	0.29%↑	1.85%↑	3.58%↑	1.83%↑	3.03%↑	1.86%↑	4.10%↑
<i>Training with 300% Mixed Synthetic Data</i>										
VideoGPT [38]	ArXiv'21	11.13	0.778	3.47	0.420	6.39	0.809	12.42	0.791	0.450
ModelScopeT2V [36]	ArXiv'23	11.18	0.775	3.42	0.425	6.31	0.815	12.20	0.797	0.456
EchoPulse [17]	ICLR'25	10.44	0.804	3.36	0.435	6.04	0.826	11.79	0.811	0.471
CardioNets [10]	NEJM AI'26	10.65	0.798	3.38	0.434	6.17	0.821	11.84	0.808	0.465
ECGFlowCMR	Ours	9.97	0.821	3.32	0.442	5.84	0.844	11.32	0.834	0.499
Increased	-	4.50%↑	2.11%↑	1.19%↑	1.61%↑	3.31%↑	2.18%↑	3.99%↑	2.84%↑	5.94%↑

**Figure 3: Ablation studies on the UKB dataset.**

importance of disentangling static anatomical structure from dynamic motion. In contrast, the full model consistently outperforms all ablated variants across evaluation metrics, demonstrating that PA-MAE and AMDF are complementary and jointly indispensable for realistic cine CMR generation.

4.5 Parameter Analysis

We further investigate the sensitivity of ECGFlowCMR to the noise scale hyperparameter α defined in Eq. 8. As depicted in Figure 4, LPIPS remains stable across varying α , whereas both FID and FVD exhibit a U-shaped response, attaining their optimal values at $\alpha = 1.0$. These results suggest that injecting an appropriate level of noise improves the distributional fidelity of the generated cine CMR sequences without compromising perceptual similarity.

**Figure 4: Parameter analysis on the UKB dataset.**

4.6 External Validations

To assess the generalizability of ECGFlowCMR beyond the UKB distribution, we conduct external validation on the ZJU-CM dataset involving both binary and four-class cardiomyopathy classification. As summarized in Table 4, model performance improves with increasing levels of synthetic augmentation up to an optimal threshold. For binary classification, the highest ACC (0.836) is achieved with 300% mixing, while the peak AUC (0.848) occurs at 400%. In the multi-class setting, the best ACC (0.745) is obtained at 400%, whereas the highest AUC (0.853) is observed at 300%. This divergence in optimal mixing levels suggests that moderate synthetic supervision enhances both discrimination and calibration, whereas excessive augmentation (e.g., 500%) may introduce distributional mismatch or redundancy, degrading downstream performance. These findings underscore the importance of balancing synthetic-to-real ratios to optimize generalization under domain shift.

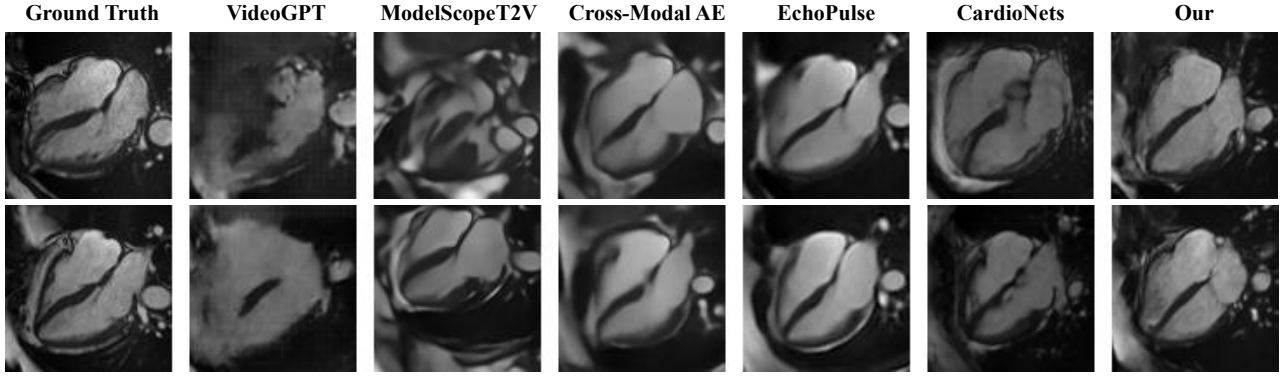


Figure 5: Comparison of synthesized CMR frames across various models.

Table 4: External validations of ECGFlowCMR on the private ZJU-CM dataset under varying synthetic-data mixing ratios.

Classification	Binary Classification		Four-Class Classification		
	Method	ACC↑	AUC↑	ACC↑	AUC↑
ViT [11]	0.736 \pm 0.038	0.671 \pm 0.061	0.531 \pm 0.022	0.694 \pm 0.055	
MAE [12](real)	0.801 \pm 0.054	0.798 \pm 0.029	0.664 \pm 0.047	0.784 \pm 0.063	
-mix 100%	0.804 \pm 0.039	0.813 \pm 0.041	0.687 \pm 0.052	0.814 \pm 0.028	
-mix 200%	0.815 \pm 0.047	0.826 \pm 0.051	0.696 \pm 0.035	0.834 \pm 0.042	
-mix 300%	0.836\pm0.027	0.843 \pm 0.029	0.717 \pm 0.054	0.853\pm0.026	
-mix 400%	0.828 \pm 0.043	0.848\pm0.059	0.745\pm0.045	0.846 \pm 0.053	
-mix 500%	0.818 \pm 0.052	0.838 \pm 0.037	0.733 \pm 0.041	0.837 \pm 0.055	

4.7 Turing Test with Cardiologists

We conducted a Turing Test with five board-certified cardiologists (one junior, three mid-level, and one senior) to evaluate the perceptual realism of cine CMR sequences synthesized by ECGFlowCMR. A total of 100 videos (50 real and 50 synthetic) were randomly selected, shuffled, and independently evaluated for binary classification (real vs. synthetic). As shown in Figure 6, the average classification accuracy was 0.514, with individual scores ranging from 0.40 to 0.60. Notably, only Expert 3 marginally exceeded chance level (0.60, 95% CI: [0.50, 0.69]), while the remaining participants performed at or near random, including Expert 5, whose accuracy was the lowest (0.40, 95% CI: [0.31, 0.50]). These findings demonstrate that ECGFlowCMR achieves high perceptual fidelity, rendering synthetic sequences nearly indistinguishable from real ones—even for experienced cardiologists. This highlights the model’s potential for clinically relevant data augmentation.

4.8 Visualization Results

Figure 5 displays representative cine CMR frames generated by different models. ECGFlowCMR yields sharper myocardial boundaries and more anatomically consistent ventricular morphology. It also better preserves temporal coherence across cardiac phases, producing smoother motion and minimizing inter-frame artifacts. Additional video results are provided in our GitHub repository.

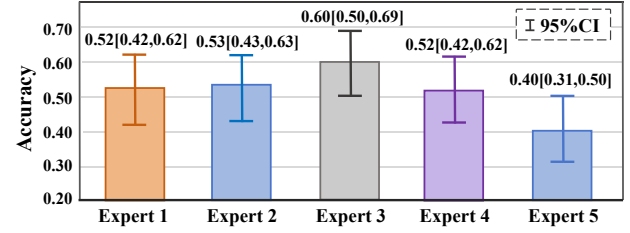


Figure 6: Performance of five cardiologists on the Turing Test. Each bar represents the classification accuracy of one cardiologist with 95% confidence intervals.

5 Limitations and Ethical Considerations

ECGFlowCMR is trained and evaluated on four-chamber cine CMR data from the UK Biobank and one external clinical cohort. Consequently, its pretraining benefits may not generalize to other imaging views, scanner vendors, clinical sites, or rare pathophysiological conditions. The use of a population-level anatomical template and latent compression ensures stable anatomy-motion synthesis but may reduce adaptability to atypical morphologies, underscoring the need for multi-center and view-diverse training. All data usage must comply with IRB approval and informed consent, including strict de-identification and access control. The generated cine CMRs are intended solely for research applications, such as augmentation and representation learning, and are not approved for standalone clinical use. Clinical oversight remains essential to mitigate risks related to misuse, bias propagation, or privacy breaches.

6 Conclusion

In this paper, we propose ECGFlowCMR, a generative framework that synthesizes realistic cine CMR sequences from 12-lead ECGs by addressing two core challenges: cross-modal temporal mismatch and anatomical observability gap. Integrating the PA-MAE and the AMDF modules, ECGFlowCMR enables scalable pretraining and improves downstream performance in cardiac classification and phenotype prediction. Extensive experiments on the UK Biobank and a proprietary clinical dataset demonstrate its quantitative and qualitative superiority over prior methods, highlighting its potential for data-efficient cardiac imaging.

GenAI Disclosure

During this research and manuscript preparation, we use Large Language Models (LLMs) for auxiliary tasks such as generating short scripts during coding and assisting with text translation and language polishing. All core ideas, research methodologies, and academic contributions are conceived and developed independently by the authors, with the role of LLMs limited to improving the fluency and readability of the presentation.

References

- [1] Salar Abbaspourazad, Oussama Elachqar, Andrew Miller, Saba Emrani, Udhayumar Nallasamy, and Ian Shapiro. 2024. Large-scale Training of Foundation Models for Wearable Biosignals. In *ICLR*.
- [2] Mohammad Babaeizadeh, Chelsea Finn, Dumitru Erhan, Roy H Campbell, and Sergey Levine. 2017. Stochastic variational video prediction. *arXiv preprint arXiv:1710.11252* (2017).
- [3] Wenjia Bai, Hideaki Suzuki, Jian Huang, Catherine Francis, Shuo Wang, Giacomo Tarroni, Florian Guilton, Nay Aung, Kenneth Fung, Steffen E Petersen, et al. 2020. A population-based genome-wide association study of cardiac and aortic structure and function. *Nature medicine* 26, 10 (2020), 1654–1662.
- [4] Andreas Blattmann, Robin Rombach, Huan Ling, Tim Dockhorn, Seung Wook Kim, Sanja Fidler, and Karsten Kreis. 2023. Align your latents: High-resolution video synthesis with latent diffusion models. In *Proceedings of the IEEE/CVF conference on computer vision and pattern recognition*. 22563–22575.
- [5] Christian Blauthgen, Pierre Chambon, Jean-Benoit Delbrouck, Rogier Van Der Sluis, Małgorzata Polacik, Juan Manuel Zambrano Chaves, Tanishq Mathew Abraham, Shivanshu Purohit, Curtis P Langlotz, and Akshay S Chaudhari. 2025. A vision–language foundation model for the generation of realistic chest x-ray images. *Nature Biomedical Engineering* 9, 4 (2025), 494–506.
- [6] Clare Bycroft, Colin Freeman, Desislava Petkova, Gavin Band, Lloyd T Elliott, Kevin Sharp, Allan Motyer, Damjan Vukcevic, Olivier Delaneau, Jared O’Connell, et al. 2018. The UK Biobank resource with deep phenotyping and genomic data. *Nature* 562, 7726 (2018), 203–209.
- [7] Tingxiu Chen, Yilei Shi, Zixuan Zheng, Bingcong Yan, Jingliang Hu, Xiao Xiang Zhu, and Lichao Mou. 2024. Ultrasound image-to-video synthesis via latent dynamic diffusion models. In *MICCAI*. Springer, 764–774.
- [8] Swakshar Deb, Nian Wu, Frederick H Epstein, and Miaomiao Zhang. 2025. Unsupervised Cardiac Video Translation Via Motion Feature Guided Diffusion Model. In *International Conference on Medical Image Computing and Computer-Assisted Intervention*. Springer, 648–658.
- [9] Emily Denton and Rob Fergus. 2018. Stochastic video generation with a learned prior. In *International conference on machine learning*. PMLR, 1174–1183.
- [10] Zhengyao Ding, Ziyu Li, Yujian Hu, Youyao Xu, Chengchen Zhao, Yiheng Mao, Haitao Li, Zhikang Li, Qian Li, Jing Wang, et al. 2024. Translating Electrocardiograms to Cardiac Magnetic Resonance Imaging Useful for Cardiac Assessment and Disease Screening: A Multi-Center Study AI for ECG to CMR Translation Study. *arXiv preprint arXiv:2411.13602* (2024).
- [11] Alexey Dosovitskiy. 2020. An image is worth 16x16 words: Transformers for image recognition at scale. *arXiv preprint arXiv:2010.11929* (2020).
- [12] Kaiming He, Xinlei Chen, Saining Xie, Yanghao Li, Piotr Dollár, and Ross Girshick. 2022. Masked autoencoders are scalable vision learners. In *CVPR*. 16000–16009.
- [13] Yingqing He, Tianyu Yang, Yong Zhang, Ying Shan, and Qifeng Chen. 2022. Latent video diffusion models for high-fidelity long video generation. *arXiv preprint arXiv:2211.13221* (2022).
- [14] Martin Heusel, Hubert Ramsauer, Thomas Unterthiner, Bernhard Nessler, and Sepp Hochreiter. 2017. Gans trained by a two time-scale update rule converge to a local nash equilibrium.
- [15] Jonathan Ho, Tim Salimans, Alexey Gritsenko, William Chan, Mohammad Norouzi, and David J Fleet. 2022. Video diffusion models. *Advances in neural information processing systems* 35 (2022), 8633–8646.
- [16] Xuan Lei, Philip Schniter, and Rizwan Ahmad. 2025. A patch-based latent video diffusion model for cardiac cine (Cine-LDiff). *Journal of Cardiovascular Magnetic Resonance* 27 (2025).
- [17] Yiwei Li, Sekeun Kim, Zihao Wu, Hanqi Jiang, Yi Pan, Pengfei Jin, Sifan Song, Yucheng Shi, Xiaowei Yu, Tianze Yang, et al. 2025. ECHOPulse: ECG Controlled Echocardiogram Video Generation. In *ICLR*.
- [18] Ziyu Li, Yujian Hu, Zhengyao Ding, Yiheng Mao, Haitao Li, Fan Yi, Hongkun Zhang, and Zhengxing Huang. 2025. Phenotype-Guided Generative Model for High-Fidelity Cardiac MRI Synthesis: Advancing Pretraining and Clinical Applications. In *MICCAI*. Springer, 484–494.
- [19] Cong Liu, Xiaohan Yuan, ZhiPeng Yu, and Yangang Wang. 2024. Texdc: Text-driven disease-aware 4d cardiac cine mri images generation. In *Proceedings of the Asian Conference on Computer Vision*. 3005–3021.
- [20] Xingchao Liu, Chengyu Gong, et al. 2023. Flow Straight and Fast: Learning to Generate and Transfer Data with Rectified Flow. In *ICLR*.
- [21] Xiaofeng Liu, Fangxu Xing, Zhangxing Bian, Tomas Arias-Vergara, Paula Andrea Pérez-Toro, Andreas Maier, Maureen Stone, Jiachen Zhuo, Jerry L Prince, and Jonghy Woo. 2024. Tagged-to-Cine MRI Sequence Synthesis via Light Spatial-Temporal Transformer. In *International Conference on Medical Image Computing and Computer-Assisted Intervention*. Springer, 701–711.
- [22] Michael Moor, Oishi Banerjee, Zahra Shakeri Hossein Abad, Harlan M Krumholz, Jure Leskovec, Eric J Topol, and Pranav Rajpurkar. 2023. Foundation models for generalist medical artificial intelligence. *Nature* 616, 7956 (2023), 259–265.
- [23] William Peebles and Saining Xie. 2023. Scalable diffusion models with transformers. In *ICCV*. 4195–4205.
- [24] Wei Peng, Ehsan Adeli, Tomas Bosscheriet, Sang Hyun Park, Qingyu Zhao, and Kilian M Pohl. 2023. Generating realistic brain mrirs via a conditional diffusion probabilistic model. In *MICCAI*. Springer, 14–24.
- [25] Eva Prakash, Jeya Maria Jose Valanarasu, Zhihong Chen, Eduardo Pontes Reis, Andrew Johnston, Anuj Pareek, Christian Blauthgen, Sergios Gatidis, Cameron Olsen, Akshay S Chaudhari, et al. 2025. Evaluating and Improving the Effectiveness of Synthetic Chest X-Rays for Medical Image Analysis. In *ICCV*. 4413–4421.
- [26] Adityanarayanan Radhakrishnan, Sam F Friedman, Shaan Khurshid, Kenney Ng, Puneet Batra, Steven A Lubitz, Anthony A Philippakis, and Caroline Uhler. 2023. Cross-modal autoencoder framework learns holistic representations of cardiovascular state. *Nature Communications* 14, 1 (2023), 2436.
- [27] Masaki Saito, Eiichi Matsumoto, and Shunta Saito. 2017. Temporal generative adversarial nets with singular value clipping. In *Proceedings of the IEEE international conference on computer vision*. 2830–2839.
- [28] Uriel Singer, Adam Polyak, Thomas Hayes, Xi Yin, Jie An, Songyang Zhang, Qiyuan Hu, Harry Yang, Oron Ashual, Oran Gafni, et al. 2022. Make-a-video: Text-to-video generation without text-video data. *arXiv preprint arXiv:2209.14792* (2022).
- [29] Petru-Daniel Tudosiu, Walter HL Pinaya, Pedro Ferreira Da Costa, Jessica Dafflon, Ashay Patel, Pedro Borges, Virginia Fernandez, Mark S Graham, Robert J Gray, Parashkev Nachev, et al. 2024. Realistic morphology-preserving generative modelling of the brain. *Nature Machine Intelligence* 6, 7 (2024), 811–819.
- [30] Sergey Tulyakov, Ming-Yu Liu, Xiaodong Yang, and Jan Kautz. 2018. Mocogan: Decomposing motion and content for video generation. In *Proceedings of the IEEE conference on computer vision and pattern recognition*. 1526–1535.
- [31] Thomas Unterthiner, Sjoerd Van Steenkiste, Karol Kurach, Raphaël Marinier, Marcin Michalski, and Sylvain Gelly. 2019. FVD: A new metric for video generation. (2019).
- [32] Aaron Van Den Oord, Oriol Vinyals, et al. 2017. Neural discrete representation learning. *Advances in neural information processing systems* 30 (2017).
- [33] Ruben Villegas, Mohammad Babaeizadeh, Pieter-Jan Kindermans, Hernan Moraldo, Han Zhang, Mohammad Taghi Saffar, Santiago Castro, Julius Kunze, and Dumitru Erhan. 2022. Phenaki: Variable length video generation from open domain textual description. *arXiv preprint arXiv:2210.02399* (2022).
- [34] Carl Vondrick, Hamed Pirsiavash, and Antonio Torralba. 2016. Generating videos with scene dynamics. *Advances in neural information processing systems* 29 (2016).
- [35] Milos Vukadinovic, Alan C Kwan, Debiao Li, and David Ouyang. 2023. GANcMRI: Cardiac magnetic resonance video generation and physiologic guidance using latent space prompting. In *Machine Learning for Health (ML4H)*. PMLR, 594–606.
- [36] Juniu Wang, Hangjie Yuan, Dayou Chen, Yingya Zhang, Xiang Wang, and Shiwei Zhang. 2023. Modelscope text-to-video technical report. *arXiv preprint arXiv:2308.06571* (2023).
- [37] Yan-Ran Wang, Kai Yang, Yi Wen, Pengcheng Wang, Yuepeng Hu, Yongfan Lai, Yufeng Wang, Kankan Zhao, Siyi Tang, Angela Zhang, et al. 2024. Screening and diagnosis of cardiovascular disease using artificial intelligence-enabled cardiac magnetic resonance imaging. *Nature Medicine* 30, 5 (2024), 1471–1480.
- [38] Wilson Yan, Yunzhi Zhang, Pieter Abbeel, and Aravind Srinivas. 2021. Videogpt: Video generation using vq-vae and transformers. *arXiv preprint arXiv:2104.10157* (2021).
- [39] Arezoo Zakeri, Alireza Hokmabadi, Ning Bi, Isuru Wijesinghe, Michael G Nix, Steffen E Petersen, Alejandro F Frangi, Zeike A Taylor, and Ali Gooya. 2023. Drag-Net: Learning-based deformable registration for realistic cardiac MR sequence generation from a single frame. *Medical Image Analysis* 83 (2023), 102678.
- [40] Oliver Zettinig, Tommaso Mansi, Dominik Neumann, Bogdan Georgescu, Saikiran Rapaka, Philipp Seegerer, Elham Kayvanpour, Farbod Sedaghat-Hamedani, Ali Amr, Jan Haas, et al. 2014. Data-driven estimation of cardiac electrical diffusivity from 12-lead ECG signals. *Medical image analysis* 18, 8 (2014), 1361–1376.
- [41] Richard Zhang, Phillip Isola, Alexei A Efros, Eli Shechtman, and Oliver Wang. 2018. The unreasonable effectiveness of deep features as a perceptual metric. In *CVPR*. 586–595.

Received 20 February 2007; revised 12 March 2009; accepted 5 June 2009